

## ROSAT EVIDENCE FOR INTRINSIC OXYGEN ABSORPTION IN COOLING FLOW GALAXIES AND GROUPS

DAVID A. BUOTE<sup>1</sup>

UCO/Lick Observatory, University of California at Santa Cruz, Santa Cruz, CA 95064; buote@ucolick.org

*Submitted to the Astrophysical Journal*

### ABSTRACT

The existence of large quantities of gas that have cooled and dropped out of the hot phase in massive elliptical galaxies, groups, and clusters is the key prediction of the inhomogeneous cooling flow scenario. Using spatially resolved, deprojected *ROSAT* PSPC spectra of 10 of the brightest cooling flow galaxies and groups with low Galactic column densities we have detected strong intrinsic absorption over energies  $\sim 0.4 - 0.8$  keV in half of the sample. Since no intrinsic absorption is indicated for energies below  $\sim 0.4$  keV, the most reasonable model for the absorber is collisionally ionized gas at temperatures  $T = 10^{5-6}$  K with most of the absorption arising from ionized states of oxygen but with a significant contribution from carbon and nitrogen. The soft X-ray emission of this warm gas can explain the sub-Galactic column densities of cold gas inferred within the central regions of most of the systems. Attributing the absorption to ionized gas reconciles the large columns of cold H and He inferred from *Einstein* and *ASCA* with the lack of such columns inferred from *ROSAT*.

Within the central  $\sim 10 - 20$  kpc, where the constraints are most secure, the estimated mass of the ionized absorber is consistent with most (perhaps all) of the matter deposited by a cooling flow over the lifetime of the flow. Since the warm absorber produces no significant H or He absorption the large absorber masses are consistent with the negligible atomic and molecular H inferred from H<sub>I</sub> and CO observations of cooling flows. It is also found that if  $T \gtrsim 2 \times 10^5$  K then the optical and UV emission implied by the warm gas does not violate published constraints. An important theoretical challenge is to understand how the warm temperature is maintained and how the gas is supported gravitationally. If magnetic pressure is responsible for the support then  $B \sim 100\mu G$  is required within the central  $\sim 5$  kpc. Finally, we discuss how the prediction of warm ionized gas as the product of mass drop-out in these and other cooling flows can be verified with new *Chandra*, *XMM*, and *ASTRO-E* observations.

*Subject headings:* cooling flows – intergalactic medium – X-rays: galaxies

### 1. INTRODUCTION

The evolution of the hot gas in the centers of massive elliptical galaxies, groups, and galaxy clusters has been most frequently interpreted in terms of the cooling flow paradigm (e.g., Fabian 1994). However, the characteristic rising temperature profiles and centrally peaked X-ray surface brightness profiles usually attributed to cooling flows can be successfully described by only assuming a two-tier structure for the gravitational potential (e.g., Ikebe et al 1996; Xu et al 1998); i.e., the cooler gas sits in the shallower potential associated with the central galaxy whereas the hotter gas sits in the deeper potential of the surrounding group or cluster. The two-tier structure is typically incorporated into cooling flow models (e.g., Thomas, Fabian, & Nulsen 1987; Brighenti & Mathews 1998), but since cooling flows are not necessarily required to explain the temperatures and surface brightness profiles of the hot gas why should they still receive attention?

Unlike the empirical two-tier potential model, cooling flows attempt to offer a nearly complete theoretical description of the time evolution of the gas properties. The energetics of a parcel of hot gas in a cooling flow is essentially governed by the balance of energy lost from radiation and energy gained from gravitational compression as the gas flows inward. Within the central regions this balance is broken as radiative cooling overwhelms gravita-

tional heating leading to the key prediction of the inhomogeneous cooling flow scenario: in massive elliptical galaxies, groups, and clusters large quantities of gas should have cooled and dropped out of the flow and be distributed at least over the central regions of the flow.

This prediction has inspired many searches in H<sub>I</sub> and CO for cold gas at the centers of cooling flows, and all such attempts have either detected small gas masses or placed upper limits which are in embarrassing disagreement with the large masses expected to have been deposited in a cooling flow (e.g., Bregman, Hogg, & Roberts 1992; O'Dea et al 1994). If instead the mass drop-out is in the form of dust then current constraints on the infrared emission in cluster cores are not inconsistent with cooling flow models (e.g., Voit & Donahue 1995; Allen et al 2000b). But cooling flows are not required to explain the infrared data in clusters (Lester et al, 1995) and individual elliptical galaxies (Tsai & Mathews, 1996).

The case for mass drop-out received a substantial boost with the discovery of intrinsic soft X-ray absorption in the *Einstein* spectral data of cooling flow clusters (White et al 1991; Johnstone et al 1992). The *Einstein* results have been verified with multitemperature models of the *ASCA* spectral data of clusters (Fabian et al 1994; Allen et al 2000b), elliptical galaxies, and groups (Buote & Fabian 1998; Buote 1999, 2000a; Allen et al 2000a). If the soft

<sup>1</sup>Chandra Fellow

X-ray absorption is interpreted as cold gas then the large intrinsic column densities of cold H suggested by the *Einstein* and *ASCA* observations still suffer from the tremendous disagreement with the H<sub>I</sub> and CO observations noted above. The *Einstein* and *ASCA* results appear even more suspect when considering that in systems with low Galactic columns no significant excess absorption from cold gas is ever found with the *ROSAT* PSPC which should be more sensitive to the absorption because of its softer bandpass, 0.1-2.4 keV (e.g., David et al 1994; Jones et al 1997; Briel & Henry 1996).

We have re-examined the *ROSAT* PSPC data of cooling flows to search for evidence of intrinsic soft X-ray absorption and in particular have allowed for the possibility that the absorber is not cold. Previously in Buote (2000c; hereafter PAPER2) we have presented temperature and metallicity profiles of the hot gas in 10 of the brightest cooling flow galaxies and groups inferred from deprojection analysis of the PSPC data. We refer the reader to that paper for details on the data reduction and deprojection procedure.

In this paper we present the absorption profiles of the 10 galaxies and groups, each of which have low Galactic column densities (see Table 1 of PAPER2). Partial results for two systems analyzed in the present paper (NGC 1399 and 5044) also appear with results for the cluster A1795 in Buote (2000b; hereafter PAPER1). In §2 we describe the models used to parameterize the soft X-ray absorption. We present the radial absorption profiles for a standard absorber model with solar abundances in §3.1. The effects of partial covering and the sensitivity of the results to the bandpass are discussed in §3.2 and §3.3. The results of modeling the absorption with an oxygen edge are presented in §3.4. We demonstrate the consistency of the *ROSAT* and *ASCA* absorption measurements in §4. Finally, in §5 we discuss in detail the implications of our absorption measurements for the physical state of the absorber, the cooling flow scenario, observations at other wavelengths, and future X-ray observations.

## 2. ABSORBER MODELS

It is standard practice to represent the soft X-ray absorption arising from the Milky Way by material with solar abundances distributed as a foreground screen at zero redshift. In this standard absorption model the X-ray flux is diminished according to  $\exp(-N_{\text{H}}\sigma(E))$ , where  $N_{\text{H}}$  is the hydrogen column density and  $\sigma(E)$  is the energy-dependent photo-electric absorption cross section for an absorber with solar abundances. We allow  $N_{\text{H}}$  to be a free parameter in our fits to indicate any excess absorption intrinsic to a galaxy or group and also to allow for any errors in the assumed Galactic value for  $N_{\text{H}}$  and for any calibration uncertainties. Note that in this standard model  $N_{\text{H}}$  is measured as a function of two-dimensional radius,  $R$ , on the sky.

Intrinsic absorption is expressed more generally as,

$$f \exp(-N_{\text{H}}\sigma[E(1+z)]) + (1-f),$$

where  $z$  is the source redshift and  $f$  is the covering factor. Since the redshifts are small for the objects in our sample any absorption in excess of the Galactic value indicated

by the standard model is essentially that of an intrinsic absorber with  $f = 1$  placed in front of the source. We discuss the effects of  $f < 1$  in §3.2.

As discussed in PAPER1 we consider oxygen absorption intrinsic to the galaxy or group which we represent by the simple parameterization of an edge,  $\exp[-\tau(E/E_0)^{-3}]$  for  $E \geq E_0$ , where  $E_0$  is the energy of the edge in the rest frame of the galaxy or group, and  $\tau$  is the optical depth. To facilitate a consistent comparison to the standard absorber model we place this edge in front of the source, and thus  $\tau$  is also measured as a function of two-dimensional radius,  $R$ , on the sky. Models with  $f < 1$  behave similarly to the solar-abundance absorber (§3.2).

The photo-electric absorption cross sections used in this paper are given by Balucińska-Church & McCammon (1992). Although Arabadjis & Bregman (1999) point out that the He cross section at 0.15 keV is in error by 13%, since we analyze  $E > 0.2$  keV we find that our fits do not change when using the Morrison & McCammon (1983) cross sections which have the correct He value. Further details on the spectral models used in the analysis are given in PAPER2.

## 3. RADIAL ABSORPTION PROFILES

Following PAPER2 we plot in Figures 1-4 the radial profiles of the column density and oxygen edge optical depth obtained from the deprojection analysis according to the number of annuli for which useful constraints on the parameters were obtained. This categorizes the systems essentially according to the S/N of the data. We refer the reader to PAPER2 for the temperature and metallicity profiles corresponding to these models.

In several cases the column densities and optical depths could not be constrained in the outermost annuli. Owing to the nature of the deprojection method large errors in the outer annuli can significantly bias the results for nearby inner annuli. Hence, in some systems we fixed the column densities to their nominal Galactic values or the edge optical depths to zero in the relevant outer annuli.

### 3.1. *Foreground Absorber with Solar Abundances*

We begin by examining the spectral fits using the standard absorption model of a foreground screen ( $z = 0$ ) with solar abundances. The left panels of Figures 1-4 show  $N_{\text{H}}(R)$  obtained from spectral fits over the energy range 0.2-2.2 keV. Our column density profiles are consistent with those presented in previous *ROSAT* studies (Forman et al 1993; David et al 1994; Trinchieri et al 1994; Kim & Fabbiano 1995; Jones et al 1997; Trinchieri et al 1997; Buote 1999) after accounting for the different plasma codes and solar abundances used.

The column densities are always within a factor of  $\sim 2$  of the Galactic value ( $N_{\text{H}}^{\text{Gal}}$ ), though in most cases  $N_{\text{H}}$  decreases as  $R$  decreases such that  $N_{\text{H}} < N_{\text{H}}^{\text{Gal}}$  at small  $R$ . For many of these systems the quality of the fit is also formally poor ( $P < 0.01$ ) in the central 1' bin, and the metallicities are very large and very inconsistent with all *ASCA* studies (see PAPER2).<sup>2</sup> Since  $N_{\text{H}} \sim N_{\text{H}}^{\text{Gal}}$  in the outer radii the observation that  $N_{\text{H}} < N_{\text{H}}^{\text{Gal}}$  at small  $R$  indicates that, whatever the origin of the deficit, it must

<sup>2</sup>Here  $P$  represents the  $\chi^2$  null hypothesis probability under the assumption of gaussian random errors. We discuss the suitability of this approximation for interpreting goodness of fit in section 3.4 of PAPER2.

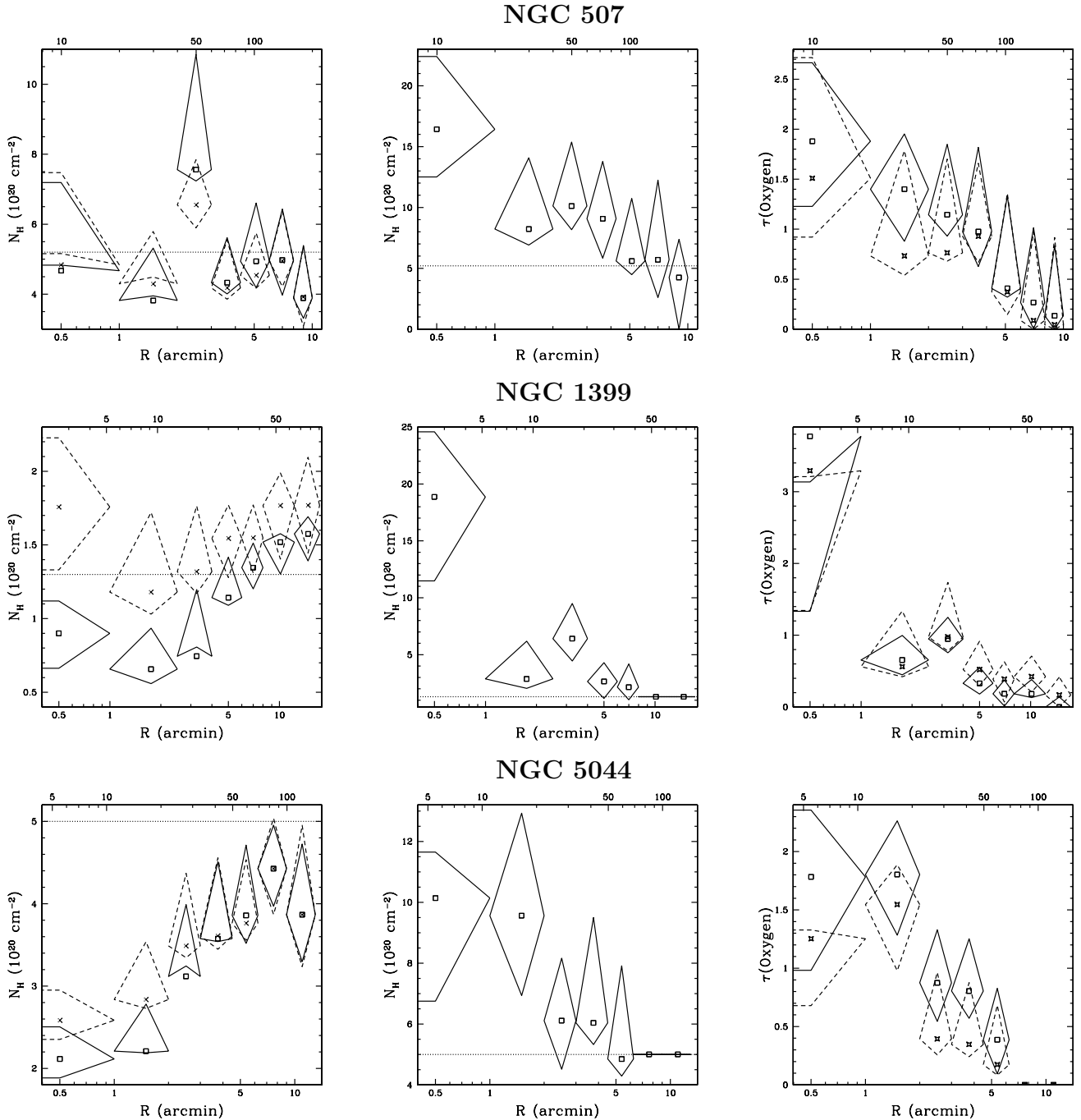


FIG. 1.— Results of the deprojection analysis for the systems where interesting constraints were obtained in 7 annuli. (Left panels) The column density profiles for a standard foreground absorber with solar abundances obtained from fits over 0.2-2.2 keV are denoted by open squares for best fit and solid diamonds for  $1\sigma$  error bars; models which also have an intrinsic oxygen edge are represented by crosses and dashed diamonds. The Galactic hydrogen column density (Dickey & Lockman, 1990) is shown as a dotted line. Radial units are arcminutes on the bottom axis and kpc on the top. (Middle panels) The column density profiles for a standard absorber obtained from fits over 0.5-2.2 keV. (Right panels) Optical depths for an oxygen edge at 0.532 keV (rest frame) obtained from fits over 0.2-2.2 keV. The open squares and solid diamonds are respectively the best fit and  $1\sigma$  errors for models where the standard absorber has  $N_H$  fixed to the Galactic value; crosses and dashed diamonds refer to models with variable  $N_H$  and thus correspond to similarly marked models in the left panels.

be intrinsic to the source. (An explanation is provided in §5.3.)

The approximately Galactic columns are wholly inconsistent with the large excess columns inferred from multi-temperature models of the *ASCA* data of these systems (Buote & Fabian 1998; Buote 1999, 2000a; Allen et al 2000a). In Buote (1999) we showed that if the lower limit of the energy range used for analysis of the PSPC data

is raised to 0.5 keV then large excess columns for NGC 1399 and 5044 consistent with the *ASCA* data are obtained. The sensitivity of  $N_H$  to the bandpass and the sub-Galactic columns argue for more complex models which we now address.

### 3.2. Effects of Partial Covering

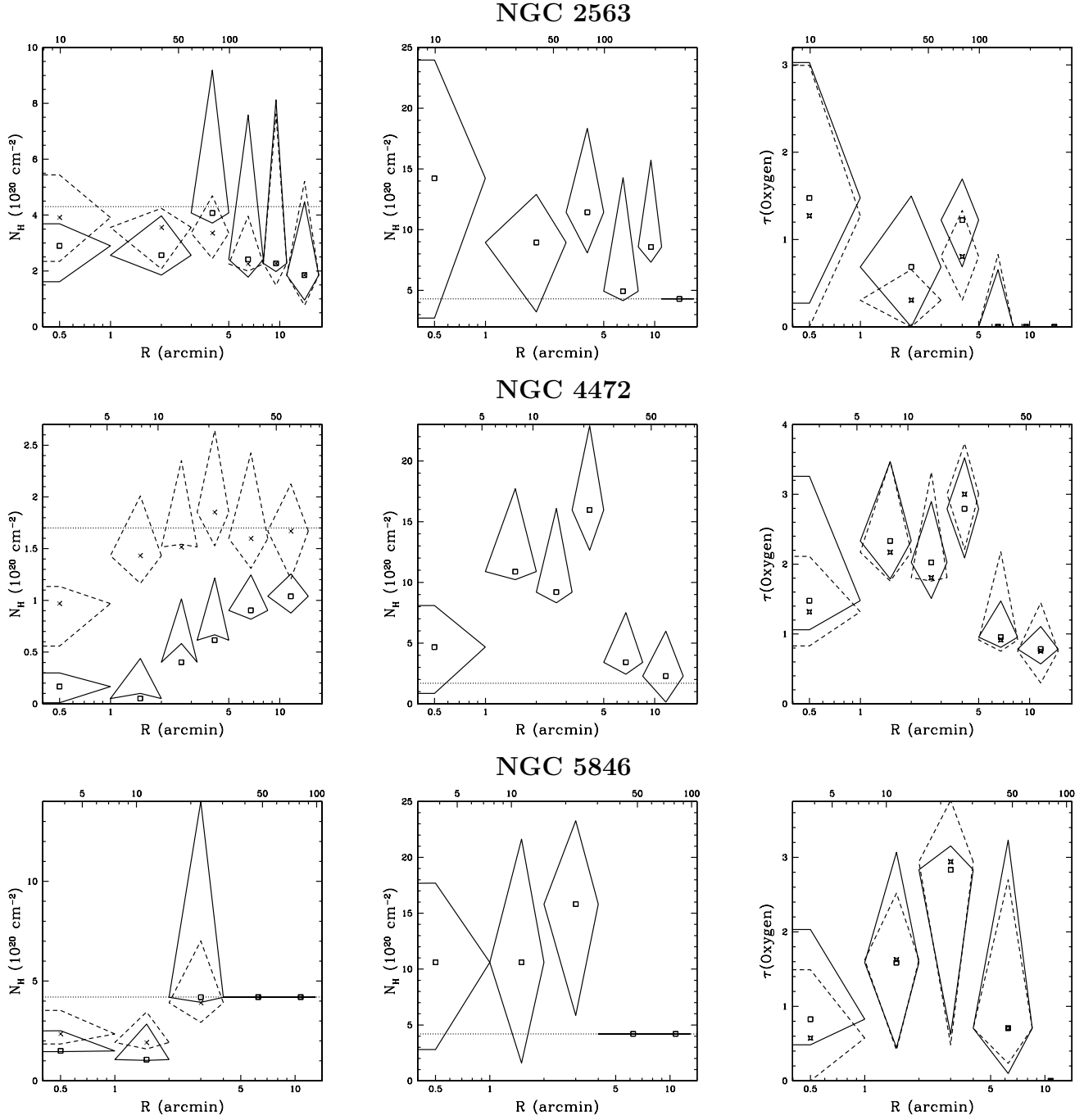


FIG. 2.— As Figure 1 but for systems with 5 or 6 annuli.

It has been suggested that the reason why analyses with the PSPC do not infer large excess column densities for cluster cooling flows is that the standard foreground model used above systematically underestimates the true column intrinsic to the system (Allen & Fabian 1996; Sarazin, Wise, & Markevitch 1998). However, in PAPER1 we have tested this hypothesis for NGC 1399 and 5044 (and the cluster A1795) using our deprojection code. We find that the hot gas within the central  $r = 1'$  (3D) cannot be absorbed very differently from the gas projected from larger radii because their spectral shapes for energies below  $\sim 0.5$  keV are very similar. If we do assume an absorber with covering factor  $f = 0.5$  we obtain an ex-

cess column  $\Delta N_H = 0$  at best fit and  $\Delta N_H < N_H^{\text{Gal}}$  at  $> 90\%$  confidence for NGC 1399 and 5044. (Note that the  $f = 0.5$  model implies a flat absorbing screen that bisects the source so that the 2D and 3D radii are equal, and thus the values of  $\Delta N_H$  quoted do refer to quantities within the 3D radius  $r = 1'$ .)

Entirely analogous results are obtained for the other systems in our sample. We mention that partial covering models never improve the fits over the  $f = 1$  case. The only effect is that somewhat larger columns are generally allowed; e.g., for  $f = 0.5$  the implied upper limits for the excess columns are typically a factor of 20%-40% larger than for  $f = 1$ .

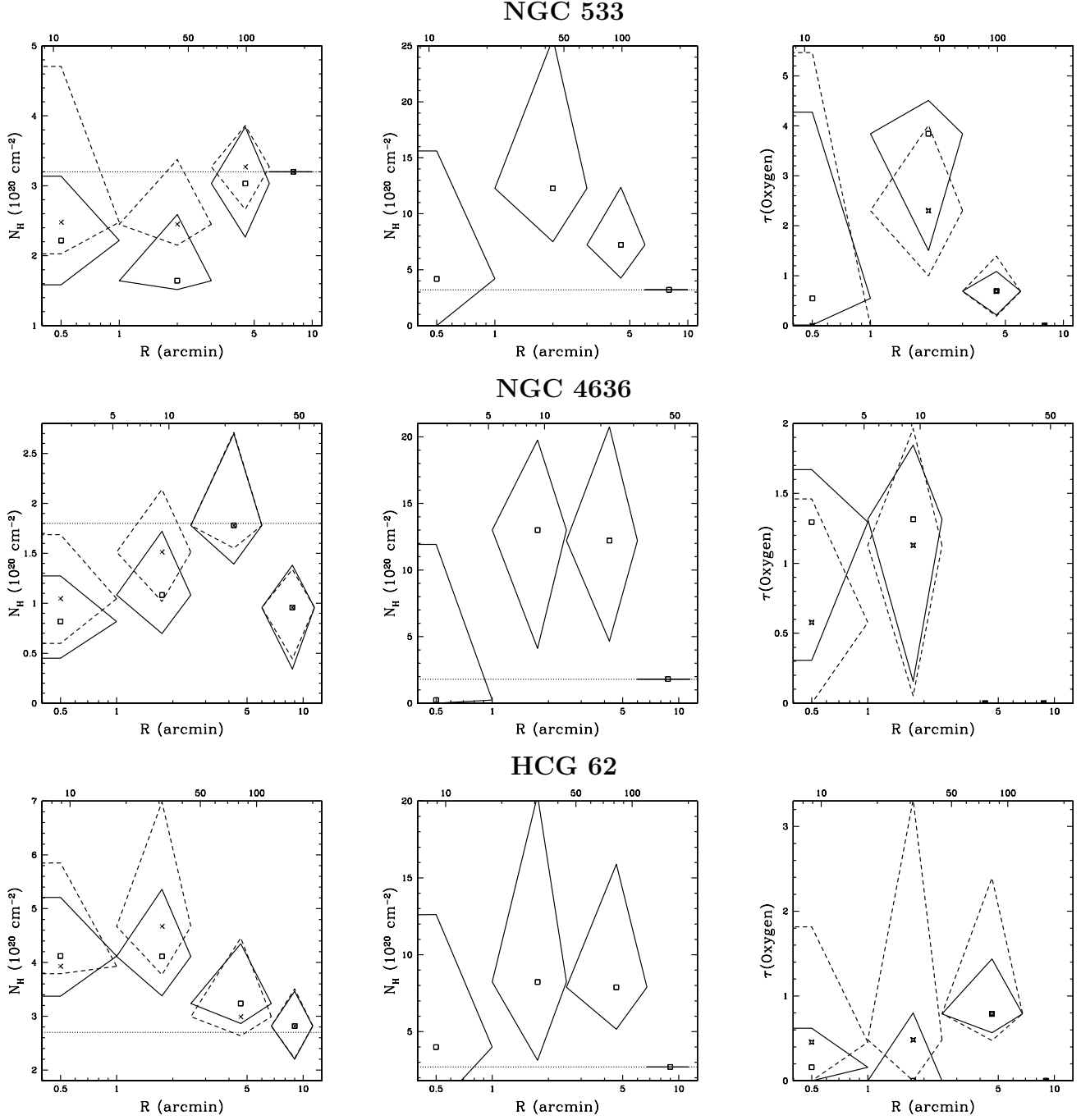


FIG. 3.— As Figure 1 but for systems with 4 annuli.

Hence, as in PAPER1 we conclude that models with  $f < 1$  cannot account for (1) the large excess columns inferred from *ASCA*, (2) the sensitivity of  $N_{\text{H}}$  to the lower energy boundary of the bandpass, or (3) the sub-Galactic columns and poor fits obtained for several systems in the central  $1'$ .

### 3.3. Sensitivity of $N_{\text{H}}(R)$ to Bandpass

As discussed in PAPER1 a solution to these discrepancies becomes transparent after examination of how  $N_{\text{H}}$  for the standard foreground model varies with the lower energy limit,  $E_{\text{min}}$ , of the bandpass within the central  $1'$ . For example when  $E_{\text{min}} \sim 0.2\text{--}0.3$  keV we find that  $N_{\text{H}} \approx N_{\text{H}}^{\text{Gal}}$

within the central bin of NGC 1399. However,  $N_{\text{H}}$  clearly increases to  $\sim 2N_{\text{H}}^{\text{Gal}}$  when  $E_{\text{min}}$  is raised to  $\sim 0.4$  keV. A dramatic change occurs when  $E_{\text{low}} \sim 0.5$  keV where  $N_{\text{H}}$  increases to several times  $N_{\text{H}}^{\text{Gal}}$  and remains essentially constant for larger  $E_{\text{min}}$ . In the middle panels of Figures 1-4 we plot  $N_{\text{H}}(R)$  for  $E_{\text{min}} = 0.5$  keV.

The character of the  $N_{\text{H}}$  profiles for  $E_{\text{min}} = 0.5$  keV is entirely different from the previous  $E_{\text{min}} = 0.2$  keV case for half of the sample: NGC 507, 1399, 4472, 4649, and 5044. In these systems  $N_{\text{H}}(R)$  for  $E_{\text{min}} = 0.5$  is consistent with the Galactic values in the outermost annuli and *increases* as  $R$  decreases until (except for NGC 4472) it reaches a value consistent with a maximum for  $R \sim 1'$ .

## NGC 4649

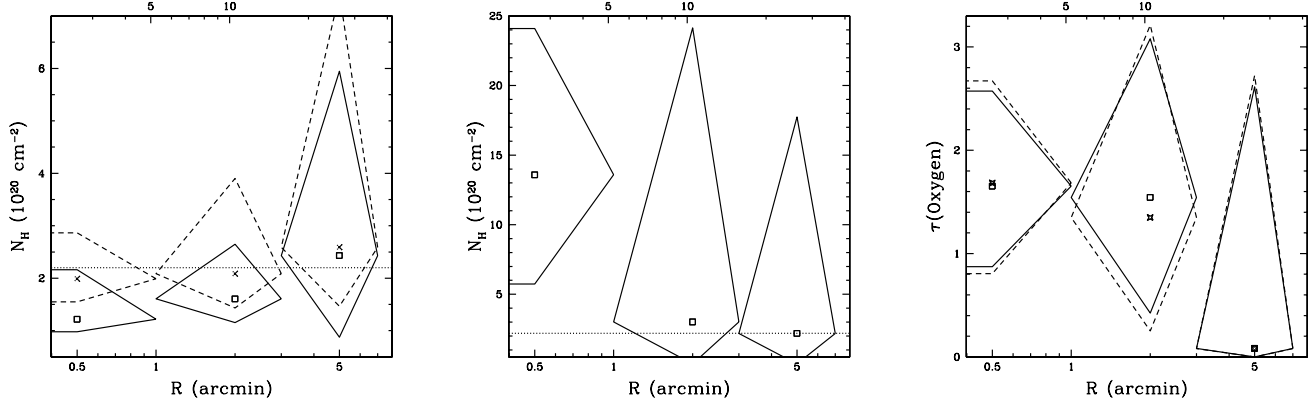


FIG. 4.— As Figure 1 but for the one system with 3 annuli.

TABLE 1  
QUALITY OF FITS AND EDGE OPTICAL DEPTH FOR  $r = 1'$

Name	$N_{\text{H}}$	No Edge			Edge		
		$\chi^2$	dof	$P$	$\chi^2$	dof	$P$
N507	Fix	36.2	47	0.87	32.2	46	0.94
	Free	34.0	46	0.91	30.4	45	0.95
N533	Fix	29.9	31	0.52	29.7	30	0.48
	Free	28.9	30	0.52	28.9	29	0.47
N1399	Fix	106.9	97	0.23	83.7	96	0.81
	Free	104.9	96	0.25	83.7	95	0.79
N2563	Fix	24.0	25	0.52	22.9	24	0.53
	Free	23.6	24	0.48	22.9	23	0.47
N4472	Fix	209.0	104	4.7E-9	158.1	103	4.0E-4
	Free	158.9	103	3.4E-4	142.2	102	5.3E-3
N4636	Fix	109.9	52	4.9E-6	105.8	51	1.0E-5
	Free	104.7	51	1.4E-5	103.1	50	1.5E-5
N4649	Fix	67.2	61	0.27	58.1	60	0.55
	Free	63.4	60	0.36	57.8	59	0.52
N5044	Fix	191.2	118	2.3E-5	156.5	117	8.7E-3
	Free	138.6	117	8.5E-2	126.4	116	0.24
N5846	Fix	84.0	47	7.4E-4	78.4	46	2.1E-3
	Free	74.6	46	4.8E-3	72.6	45	5.7E-3
H62	Fix	37.8	46	0.80	37.7	54	0.77
	Free	38.6	45	0.74	37.7	44	0.74

NOTE.—Results of deprojection analysis in the central radial bin ( $R = 1'$ ). Models where the column density of the standard foreground absorber with solar abundances is fixed to the Galactic value are indicated by “Fix” under the  $N_{\text{H}}$  column; variable column models are indicated by “Free”. For the models with an intrinsic oxygen edge at 0.532 keV (rest frame) we list the best-fitting optical depth,  $\tau$ , with its 95% confidence lower limit in parentheses. The  $\chi^2$  null hypothesis probability is listed in the column  $P$  under the assumption of gaussian random errors (see section 3.4 of PAPER2).

For the other five galaxies the constraints are too poor to discern a trend, though within the large errors their profiles are consistent with increasing as  $R \rightarrow 0$ .

### 3.4. Intrinsic Oxygen Edge

Since we find that  $N_{\text{H}}(E_{\text{min}}) \approx \text{constant}$  for  $E_{\text{min}} > 0.5$  keV, the portion of the spectrum responsible for the excess absorption must be near 0.5 keV. Considering the PSPC resolution and effective area this translates to energies  $\sim 0.4 - 0.7$  keV. The dominant spectral features in both absorption and emission over this energy range are due to oxygen, though ionized carbon and nitrogen can contribute as well (see §5.1). Since the PSPC data cannot distinguish between a single edge and multiple edges, we parameterize the intrinsic absorption with an edge at

0.532 keV (rest frame) corresponding to cold oxygen ( $\text{O I}$ ). In the right panels of Figures 1-4 we plot the optical depth profiles,  $\tau(R)$ , for the  $\text{O I}$  edge obtained from fits over 0.2-2.2 keV.

For every system we find that the shape of  $\tau(R)$  is very similar to that of  $N_{\text{H}}(R)$  for  $E_{\text{min}} = 0.5$  for the standard absorber. Moreover, for those systems where  $N_{\text{H}} \gg N_{\text{H}}^{\text{Gal}}$  for  $E_{\text{min}} = 0.5$  we find that  $\tau(R) \lesssim 0.1$  in the outermost annuli and increases to  $\tau(R) \sim 1$  in the central bin. Thus, the oxygen edge by itself reproduces all of the excess absorption required by  $N_{\text{H}}(R)$  for  $E_{\text{min}} = 0.5$  for the standard absorber model.

In NGC 507, 1399, 4472, 4649, and 5044 the edge significantly improves the fits in the central bin (Table 1). Only for these systems is  $\tau > 0$  significant at the 95% con-

fidence level in the central bin. Both of these results apply whether or not  $N_{\text{H}}$  is fixed to the Galactic value for the standard absorber model.

For every system where we found  $N_{\text{H}} < N_{\text{H}}^{\text{Gal}}$  for the standard absorber (§3.1), we find that  $N_{\text{H}}$  systematically increases when the oxygen edge is added. Although the addition of the edge results in  $N_{\text{H}} \sim N_{\text{H}}^{\text{Gal}}$  for many of these systems we find that in some cases (e.g., NGC 5044)  $N_{\text{H}}$  is still significantly less than  $N_{\text{H}}^{\text{Gal}}$ , and the fits in the central bin, though improved, are still formally unacceptable. Thus, adding the edge does significantly improve the models, but it apparently is not the only improvement required in some cases (see §5.3).

If instead we allow the oxygen abundance in the hot gas to be a free parameter in the fits we find that typically the best-fitting oxygen abundance is zero, and the quality of most of the fits are improved similarly to that found when the oxygen edge is added. This degeneracy is not surprising owing to the limited energy resolution of the PSPC. The notable exception is NGC 1399 where the fits for  $r = 1'$  are only improved to  $\chi^2 = 95.9$  for zero oxygen abundance as opposed to 83.7 for the edge (both have variable  $N_{\text{H}}$ ). However, zero oxygen abundance in the centers is highly unlikely because of the expected enrichment from the stars in the central galaxy. And if instead we consider plausible O/Fe ratios to be at least 1/2 solar in NGC 507, 1399, 4472, 4649, and 5044, then the fits are not as much improved as when adding the edge.

As mentioned above (and in PAPER1) we find that for most radii the constraints on the edge energy are not very precise which is why we fixed the edge energy in our analysis. The best constraints are available for NGC 1399 and 5044 within the central bin for which we obtain  $0.51^{+0.05}_{-0.05}$  keV and  $0.51^{+0.09}_{-0.05}$  keV (90% confidence) for the edge energies for the standard absorber models with variable  $N_{\text{H}}$ . (Models with fixed foreground Galactic columns give similar results; e.g.,  $0.53^{+0.05}_{-0.03}$  keV for NGC 1399.)

These constraints are consistent with the lower ionization states of oxygen but not edges from the highest states O vi-viii. Due to the limited resolution we can add additional edges to “share” the  $\tau$  obtained for the O<sub>1</sub> edges, although when using a two-edge model a significant  $\tau$  cannot be obtained for edge energies above  $\sim 0.65$  keV corresponding to  $\sim \text{O vi}$ .

### 3.5. Comments on Individual Systems

We elaborate further on the results for individual systems. When comparing  $N_{\text{H}}$  profiles to those obtained from previous *ROSAT* PSPC studies we implicitly any differences in the plasma codes and solar abundances used.

#### 3.5.1. Systems with 7 Annuli

In Figure 1 we display the results for the three systems where the spectral parameters are well determined in seven annuli. These observations thus generally correspond to the highest S/N data in our sample. The evidence for intrinsic oxygen absorption is strongest for these systems.

**NGC 507:** The oxygen edge optical depth,  $\tau(R)$ , falls gradually from the center and remains significantly non-zero out to  $R \sim 4'$ ; e.g., in the  $R = 3'$ - $4.25'$  annulus the 95% confidence lower limits on  $\tau$  are 0.39 and 0.24 respectively in models with fixed (Galactic) and variable  $N_{\text{H}}$  for

the standard absorber. The values of  $N_{\text{H}}$  for the standard absorber are consistent with those obtained by Kim & Fabbiano (1995) with the PSPC data.

**NGC 1399:** This system exhibits the most centrally peaked  $\tau$  profile in our sample. Within the central arcminute  $\tau > 0.26$  and 0.33 at 99% confidence respectively for the fixed and free  $N_{\text{H}}$  models. At larger radii the non-zero optical depths are also quite significant; e.g., for  $R = 2.5'$ - $4'$   $\tau > 0.64$  and 0.50 at 99% confidence for the fixed and free  $N_{\text{H}}$  models. We obtain values of  $N_{\text{H}}$  for the standard absorber consistent with the previous PSPC study by Jones et al (1997).

**NGC 5044:** The second radial bin ( $R = 1'$ - $2'$ ) actually has a smaller uncertainty on the oxygen edge optical depth than the central bin; i.e., the 95% lower limits on  $\tau$  are 0.87 and 0.79 respectively for the fixed and free  $N_{\text{H}}$  models. In fact, the corresponding 99% lower limits are 0.75 and 0.42 for  $R = 1'$ - $2'$  which are larger than the values for the  $R = 1'$  bin. The optical depth remains significantly non-zero out to the  $R = 3'$ - $4.5'$  bin in which we obtain 95% lower limits on  $\tau$  of 0.36 and 0.10 for the fixed and free  $N_{\text{H}}$  models. Our values of  $N_{\text{H}}$  are consistent with those obtained from PSPC data by David et al (1994).

#### 3.5.2. Systems with 5-6 Annuli

In Figure 2 we display the results for the three systems where the spectral parameters are well determined in 5-6 annuli. Only for NGC 4472 is the intrinsic oxygen absorption clearly significant.

**NGC 2563:** The uncertainties on  $\tau(R)$  are large and consistent with zero at the center. However, the shapes of the error regions, especially the large uncertainty at the center, are consistent with the same type of increasing  $\tau$  profile with decreasing  $R$  found for the systems with seven annuli.

**NGC 4472:** The optical depth is consistent with  $\tau \sim 2$  for  $R \lesssim 5'$  and then decreases rapidly at larger radii. Unlike the other systems with evidence for intrinsic absorption  $\tau$  is most significant away from the central bin; i.e., for  $R = 3.25'$ - $5'$  the 95% confidence lower limits on  $\tau$  are 1.62 and 1.75 respectively for the fixed and free  $N_{\text{H}}$  models. (The corresponding 99% lower limits are 1.27 and 1.46.) Interestingly,  $R \sim 5'$  corresponds to the region where Irwin & Sarazin (1996) identified holes in the X-ray emission from visual examination of the PSPC image, and thus the large oxygen edge optical depths could be related to these holes. The sub-Galactic columns obtained for the standard absorber with variable  $N_{\text{H}}$  are consistent with those obtained by Forman et al (1993).

**NGC 5846:** The uncertainties on  $\tau(R)$  are large, and although a substantial amount of intrinsic absorption is allowed by the data, no excess absorption is required.

#### 3.5.3. Systems with 4 Annuli

In Figure 3 we display the results for the three systems where the spectral parameters are well determined in 4 annuli. The uncertainties on  $\tau(R)$  are large for each of these systems and thus no intrinsic oxygen absorption is clearly required by the data.

#### 3.5.4. Systems with 3 Annuli

In Figure 4 we display the results for the one system where the spectral parameters are well determined in only

3 annuli, NGC 4649. In contrast to the systems with 4 annuli we find evidence for significant intrinsic oxygen absorption in the central bin for NGC 4649.

**NGC 4649:** In the central radial bin the 90% lower limits on  $\tau$  are 0.55 and 0.20 respectively for the fixed and free  $N_{\text{H}}$  models, although only the 95% lower limit for the model with fixed  $N_{\text{H}}$  is significantly larger than zero (Table 1). Our values of  $N_{\text{H}}$  for the standard absorber are consistent with those obtained from the PSPC data by Trinchieri et al (1997).

### 3.6. Caveats

(i) *Calibration:* The gain of the PSPC is well calibrated and in particular no significant calibration problems near 0.5 keV have been reported.<sup>3</sup> The large values of  $\tau \sim 1$  obtained in the central regions imply that the absorption significantly effects a large energy range comparable to the energy resolution of the PSPC; e.g., the O<sub>1</sub> edge absorbs 25% of the flux at 0.8 keV for  $\tau = 1$ ; i.e. possible residual calibration errors near 0.5 keV where the effective area is changing rapidly (e.g., Figure 1 of Snowden et al 1994) can not explain the need for absorption at higher energies. Moreover, the shape of  $\tau(R)$  is not the same for each system as would be expected if calibration were responsible for the intrinsic oxygen absorption found in half of the sample; e.g.,  $\tau(R)$  for NGC 1399 is much more centrally peaked than for NGC 4472 or the other systems. The agreement between the absorption inferred by the PSPC and ASCA mentioned below in §4 further argues against a systematic error intrinsic to the PSPC being responsible for the measured oxygen absorption.

(ii) *Galactic Columns:* All of the objects in our sample reside at high Galactic latitude, and thus the Galactic absorption should be very uniform over the relevant 5'-10' scales. Errors in the assumed Galactic columns (Dickey & Lockman, 1990) should only affect the baseline value and not the variation with radius.

(iii) *Background:* Errors in the background level affect most seriously the lowest energies ( $\lesssim 0.4$  keV) which are also most sensitive to the column density of the standard absorber model. Hence, measurements of  $N_{\text{H}}$  at the largest radii (which have lowest S/N) are the most affected by background errors. The hydrogen column densities measured in the outer radii (see Figures 1-4) are very similar to and are usually consistent with the assumed Galactic values within the estimated  $1\sigma$  errors which attests to the accuracy of our background estimates. The intrinsic oxygen optical depths in the central radial bins are very insensitive to the background level.

(iv) *Single-Phase Gas:* As we mentioned in PAPER2 multiphase models of the hot gas are not required by the PSPC data. The intrinsic absorption predicted by two-phase and cooling flow models is mostly consistent with that of the single-phase models. The cooling flow models in some cases require even more intrinsic oxygen absorption (about a factor of two) because such models generate stronger oxygen lines than do the single-phase models.

## 4. COMPARISON TO ASCA

The intrinsic oxygen absorption indicated by the PSPC data in half of our sample is most significant within the

central 1' – 2' which is similar to the width of the ASCA PSF. In addition, since the ASCA SIS is limited to  $E > 0.5$  keV, and the efficiency near 0.5 keV is severely limited due to instrumental oxygen absorption, it cannot be expected that ASCA can distinguish an oxygen edge from a standard absorber with solar abundances. However, it is instructive to examine the consistency between results obtained from spatially resolved (PSPC) and single-aperture (ASCA) methods. As mentioned in PAPER1 the results obtained when adding an oxygen edge to the ASCA data of NGC 1399 and 5044 are entirely consistent with those obtained with the PSPC. Since similar results are found for all the objects in our sample, we focus on NGC 1399 for illustration.

Previously we (Buote, 1999) have fitted two-temperature models to the accumulated ASCA SIS and GIS data within  $R \approx 5'$  of NGC 1399 and obtained  $N_{\text{H}}^{\text{c}} = 49_{-9}^{+6} \times 10^{20} \text{ cm}^{-2}$  (90% confidence) for the standard absorber on the cooler temperature component. Using the meteoritic solar abundances (see §4.1.3 of PAPER2) slightly modifies this result to  $N_{\text{H}}^{\text{c}} = 40_{-7}^{+6} \times 10^{20} \text{ cm}^{-2}$  which is consistent with the total column within  $R \approx 5'$  obtained from the PSPC for  $E_{\text{min}} = 0.5$  keV (Fig 1). If instead the columns of the standard absorber are fixed to Galactic on both components, and an intrinsic O<sub>1</sub> edge is added to the cooler component, then we obtain  $\tau = 6.0_{-0.7}^{+0.7}$  (90% confidence) for the ASCA data. This is very consistent with the value of  $\tau = 5.7$  obtained from adding up the best-fitting values obtained with the PSPC within  $R = 5'$ . Therefore, the oxygen edge provides as good or better description of the excess absorption inferred from multitemperature models of ASCA data within the central few arcminutes as a standard cold absorber with solar abundances, and yields optical depths that are consistent with those obtained with the PSPC data.

Although a similar consistency is achieved for NGC 4472 the interpretation of the absorption of the two-component model of the single-aperture ASCA data is not so straightforward because the absorption is not obviously concentrated at the center (i.e. on the cooler temperature component). In fact, a spatially uniform absorber within  $R = 5'$  is probably a better description of the PSPC data. If the column densities on both temperature components are tied together for the two-temperature model of the ASCA data the quality of the fit is slightly worse ( $\Delta\chi^2 = 8$  for 361 dof), but  $N_{\text{H}} \approx 11 \times 10^{20} \text{ cm}^{-2}$  which is a fair representation of the average  $N_{\text{H}}$  profile obtained from the PSPC for  $E_{\text{min}} = 0.5$  keV (Fig 2). Similar agreement is found for the O<sub>1</sub> edge when applied to both temperature components.

## 5. DISCUSSION AND CONCLUSIONS

From deprojection analysis of the ROSAT PSPC data of 10 cooling flow galaxies and groups with low Galactic columns we have detected strong oxygen absorption intrinsic to the central  $\sim 1'$  in half of the sample: NGC 507, 1399, 4472, 4649, and 5044. The data for the other systems are insufficient to place interesting constraints on the absorption profile but are consistent with substantial absorption. We modeled the oxygen absorption as an edge (rest frame  $E = 0.532$  keV) which produces the necessary absorption in both the PSPC and ASCA data for  $E \gtrsim 0.5$

<sup>3</sup>See <http://heasarc.gsfc.nasa.gov/docs/rosat>.

keV without violating the PSPC constraints over  $0.2 \sim 0.4$  keV for which no significant excess absorption is indicated.

The intrinsic oxygen absorption reconciles the long-standing problem of why negligible column densities for a foreground absorber with solar abundances were inferred from *ROSAT* data whereas large columns were obtained from *ASCA* and other instruments with bandpasses above  $\sim 0.5$  keV. Moreover, since the absorption is confined to energies above  $\sim 0.5$  keV there is no need for large columns of cold H which are known to be very inconsistent with the negligible atomic and molecular H measured in galactic and cluster cooling flows (e.g., Bregman et al 1992; O'Dea et al 1994).

The limited energy resolution of the PSPC does not place tight constraints on the energy of the oxygen edge or the number of edges. For a single edge we obtain  $E \approx 0.45$ – $0.6$  keV corresponding to ionization states O<sub>1</sub>–v. Models with two edges allow for slightly higher edge energies  $\sim 0.65$  keV which are consistent with ionization states up to O<sub>vi</sub>.

### 5.1. Warm Ionized Gas

Dust is unlikely to be a significant contributor to the intrinsic X-ray absorption because dust should not contain carbon or oxygen since CO is expected to be evaporated off of dust grains by X-ray heating (e.g., Voit & Donahue 1995). Moreover, dust is rapidly sputtered away in the centers of galactic cooling flows (e.g., Tsai & Mathews 1995; Voit & Donahue 1995) where the soft X-ray absorption is most significant. Hence, the most reasonable state for the intrinsic absorbing material is that of warm, collisionally ionized gas. The requirement that H and He be completely ionized implies that  $T \gtrsim 1.0 \times 10^5$  K (e.g., Sutherland & Dopita 1993), whereas the maximum temperature which can give rise to significant absorption at 0.5 keV is  $\approx 1 \times 10^6$  K (see Figure 2 of Krolik & Kallman 1984).

At these temperatures carbon and nitrogen are not completely ionized (e.g., Nahar & Pradhan 1997; Sutherland & Dopita 1993), and thus these elements will also contribute to the soft X-ray absorption. For nitrogen the states N<sub>IV</sub>–vi are significant, and their edge energies span 0.46–0.55 keV (rest frame) which are consistent with the edge energy range determined from the PSPC data. Since N/O = 1/8.51 (assuming solar abundance ratios), and the threshold cross sections for absorption are similar for N and O, only  $\sim 12\%$  of the optical depth we have measured in each system likely arises from ionized nitrogen.

The ionization fraction for carbon changes rapidly near  $T = 10^5$  K with Cv dominating for temperatures above this value and up to  $T \approx 10^6$  K. The edge energy for Cv is 0.39 keV, and since C/O  $\approx 0.5$  (assuming solar abundance ratios) and the threshold cross sections of C and O are similar, the optical depth of Cv is about half that expected from a dominant ionized state of oxygen. However, the strong instrumental carbon absorption leaves the PSPC with essentially no effective area over energies 0.28 keV to  $\sim 0.4$  keV (e.g., see Figure 1 of Snowden et al 1994), and thus it is only possible to detect intrinsic absorption from the Cv edge for energies above  $\sim 0.4$  keV even considering the smearing due to the limited energy resolution. This is entirely consistent with the variation of  $N_{\text{H}}$  with  $E_{\text{min}}$  described in §3.3.

Considering the energy resolution and effective area curve of the PSPC, the 0.532 keV edge that we have used to parameterize the intrinsic absorption is likely an average of the  $\sim 40\%$  contribution from the Cv edge (0.39 keV) and N<sub>IV</sub>–vi edges (0.46–0.55 keV) with a  $\sim 60\%$  contribution from ionized oxygen states. Although as discussed in §3.4 the PSPC data cannot distinguish between multi-edge models, when using a more realistic absorber model consisting of Cv and N<sub>vi</sub> and an oxygen edge, we are able to obtain a significant optical depth for the oxygen edge for energies as high as  $\sim 0.75$  keV consistent with O<sub>vii</sub> (0.74 keV). However, to insure that oxygen produces at least as much absorption as the C and N edges, the PSPC data also require a contribution from edges around  $\sim 0.6$ – $0.65$  keV corresponding to edges from O<sub>IV</sub>–vi.

Consideration of these maximum allowed ionization states for oxygen indicates that the maximum temperature of the warm gas is more like  $T \approx 5 \times 10^5$  K (e.g., Nahar 1999; Sutherland & Dopita 1993). The absorption signature from this warm gas is not one dominant feature near 0.5 keV but is rather a relatively broad trough over energies 0.4 to  $\sim 0.8$  keV for total optical depths of unity (see Figure 1 of Krolik & Kallman 1984).

(We mention that the edge energies we have quoted are from Daltabuit & Cox (1972) though Gould & Jung (1991) argue that the edge energy for O<sub>1</sub> is  $\sim 10$  eV higher. Such differences may be relevant for modeling future high resolution spectra but are unimportant for our present discussion with the PSPC data.)

### 5.2. Absorber Masses and Cooling Flows

As suggested in PAPER1 this warm ionized absorber might be the gas that has dropped out of the putative cooling flow during the lifetime of the galaxy or group and thus could provide the confirmation of the inhomogeneous cooling flow scenario that has been suggested to operate in massive elliptical galaxies, groups, and clusters (e.g., Fabian 1994). To make this connection between our measurements of oxygen absorption and the cooling flow scenario we first estimate the mass of absorbing material implied by the measured optical depths. This mass is then compared to the cooling flow mass deposition rate inferred from *ASCA* data.

Assuming the optical depths refer to the O<sub>1</sub> edge, then the measured values of  $\tau$  imply a hydrogen column density (assuming  $\sigma = 5.5 \times 10^{-19} \text{ cm}^{-2}$  at threshold) and thus a mass within a projected radius,  $R$ ,

$$M_{\text{abs}}(< R) = (7.8 \times 10^9)(\tau) \left( \frac{R}{10 \text{kpc}} \right)^2 \left( \frac{\text{O/H}}{8.51 \times 10^{-4}} \right)^{-1} M_{\odot}, \quad (1)$$

where  $\tau$  is the optical depth of the O<sub>1</sub> edge and O/H is the oxygen abundance of the absorber. Although the projected mass is larger than the mass within the 3D radius  $r = R$ , the value of  $\tau$  in equation (1) slightly underestimates the 3D value as discussed in (§3.2); i.e. these projection effects approximately cancel. The metallicity of the hot gas in the central bins for the objects in our sample are larger than solar (PAPER2), and thus we expect the same for the absorber. Since the oxygen abundance is uncertain we shall quote results assuming O is solar and recognize

TABLE 2  
ABSORBER MASSES AND IMPLIED ACCUMULATION TIMESCALES

Name	Central Bin				Total				
	$\dot{M}$ ( $M_{\odot} \text{yr}^{-1}$ )	R (kpc)	$M_{\text{abs}}$ ( $10^{10} M_{\odot}$ )	$t_{\text{acc}}$ ( $10^{10} \text{yr}$ )	$M_{\text{hot}}$ ( $10^{10} M_{\odot}$ )	R (kpc)	$M_{\text{abs}}$ ( $10^{10} M_{\odot}$ )	$t_{\text{acc}}$ ( $10^{10} \text{yr}$ )	$M_{\text{hot}}$ ( $10^{10} M_{\odot}$ )
N507	$18.50^{+3.50}_{-3.30}$	20.0	$5.86^{+5.85}_{-4.02}$	$0.32^{+0.45}_{-0.23}$	$0.430^{+0.221}_{-0.069}$	200.0	$125.67^{+599.92}_{-92.61}$	$6.79^{+40.94}_{-5.29}$	$43.68^{+12.31}_{-9.41}$
N1399	$1.62^{+0.20}_{-0.18}$	5.2	$0.81^{+0.16}_{-0.62}$	$0.50^{+0.13}_{-0.39}$	$0.019^{+0.012}_{-0.001}$	90.3	$9.41^{+23.11}_{-7.10}$	$5.81^{+16.78}_{-4.54}$	$5.55^{+0.51}_{-0.63}$
N4472	$2.54^{+0.34}_{-0.37}$	5.2	$0.32^{+0.54}_{-0.16}$	$0.12^{+0.27}_{-0.07}$	$0.031^{+0.002}_{-0.018}$	77.2	$47.26^{+39.53}_{-24.67}$	$18.61^{+21.39}_{-10.76}$	$3.65^{+0.36}_{-0.33}$
N4649	$2.20^{+0.90}_{-0.60}$	5.2	$0.35^{+0.41}_{-0.26}$	$0.16^{+0.32}_{-0.13}$	$0.026^{+0.004}_{-0.014}$	36.7	$3.70^{+60.64}_{-3.61}$	$1.68^{+38.53}_{-1.65}$	$0.56^{+0.19}_{-0.25}$
N5044	$41.32^{+4.59}_{-5.42}$	11.0	$1.69^{+1.17}_{-1.13}$	$0.04^{+0.04}_{-0.03}$	$0.266^{+0.052}_{-0.109}$	143.5	$26.52^{+38.17}_{-17.87}$	$0.64^{+1.16}_{-0.45}$	$22.08^{+2.91}_{-4.13}$

NOTE.—Total cooling flow mass deposition rates ( $\dot{M}$ ) and 90% confidence limits inferred from *ASCA* data (see text). The quoted errors on  $M_{\text{abs}}$  refer to 95% confidence limits and assume solar abundances. The accumulation timescale,  $t_{\text{acc}} = M_{\text{abs}}/\dot{M}$ , reflects both the 95% uncertainties on  $M_{\text{abs}}$  and the 90% errors on  $\dot{M}$ . The mass of hot gas,  $M_{\text{hot}}$ , and the 95% errors computed within the 3D radius are also given.

that  $M_{\text{abs}}$  could be overestimated by a factor of 2-3 in the central bin. The expected contribution from carbon and nitrogen (§5.1) to  $\tau$  also reduces  $M_{\text{abs}}$  by another  $\sim 40\%$ .

In Table 2 we give  $M_{\text{abs}}$  for NGC 507, 1399, 4472, 4649, and 5044 in both the central bin ( $R = 1'$ ) and the total mass interior to the largest bin investigated. The mass deposition rates,  $\dot{M}$ , listed in the second column are determined from the accumulated *ASCA* data within radii of  $r \sim 3' - 5'$ . (The *ASCA* spectra place much tighter constraints on the total  $\dot{M}$  than do the *ROSAT* spectral data.) The results for NGC 1399, 4472, and 5044 are taken from Buote (1999). For NGC 507 and 4649 we re-analyzed the data sets as prepared in Buote & Fabian (1998) and fitted cooling flow models analogously to that done in Buote (1999). That is, the spectra were fitted with (1) a constant pressure cooling flow component, (2) an isothermal component representing the ambient gas, and (3) for NGC 4649 an extra high-temperature bremsstrahlung component. Since the cooling flow model assumes constant pressure and neglects the gravitational work done on the cooling gas, the value of  $\dot{M}$  is an upper limit. This overestimate is typically  $\lesssim 30\%$  (e.g., the agreement of different cooling flow models in Allen et al 2000b).

Let us focus on  $M_{\text{abs}}$  and the accumulation time,  $t_{\text{acc}} = M_{\text{abs}}/\dot{M}$ , within the central bin ( $R = 1'$ ) where the measured optical depths are most significant and the fits are most clearly improved when the edge is added; i.e. we consider the results for the central bin to be most reliable. Assuming an age of the universe,  $t_{\text{age}} = 13 \times 10^{10} \text{yr}$ , examination of Table 2 reveals that within the central bin  $t_{\text{acc}} \sim (0.1 - 0.5)t_{\text{age}}$  using the best-fitting values or a 95% upper limit of  $t_{\text{acc}} \sim (0.3 - 0.6)t_{\text{age}}$ ; NGC 5044 actually has smaller values, but if the second bin is included (which has intrinsic absorption just as significant as the inner bin) then  $t_{\text{acc}}$  is consistent with the values quoted above. These accumulation timescales are a sizeable fraction of  $t_{\text{age}}$ , and thus  $M_{\text{abs}}$  within the central bin(s) can account for most, if not all, of the mass deposited by the cooling flow over the lifetime of the flow; the exact value depends on precisely when the cooling flow begins and whether  $\dot{M}$  varies with time.

The total absorbing masses have large errors within the 95% confidence limits. Although the best-fitting values for

$t_{\text{acc}}$  are typically larger than  $t_{\text{age}}$ , the 95% lower limits are  $\lesssim t_{\text{age}}$  for all but NGC 4472. We reiterate that we consider these values at the largest radius to be less secure than the central bin(s) because the fits do not clearly require the addition of the oxygen edge outside the inner 1-2 bins. Nevertheless, the result for NGC 4472 is striking and deserves comment. Clearly the approximation of a spherically symmetric, relaxed cooling flow is invalid for  $R \gtrsim 3'$  because the isophotal distortions suggest a strong interaction with the surrounding Virgo gas (Irwin & Sarazin, 1996) and thus the estimate of  $\dot{M}$  unlikely applies at larger radii. If the large value of  $M_{\text{abs}}$  at large radius is confirmed then another mechanism must have produced the warm gas in NGC 4472.

Hence, within the central 1-2 bins ( $R \sim 10 - 20 \text{kpc}$ ) where the model constraints are most secure we conclude that the absorbing mass inferred from the oxygen edges can explain most (and perhaps all) of the mass deposited by a cooling flow over the age of the system. If the edges also apply at larger radii (as we have assumed), then all of the deposited mass (except for NGC 4472) can be easily explained by the inferred absorbing mass.

### 5.3. X-Ray Emission from the Warm Gas

Recall that when fitted with only a standard absorber with solar abundances that  $N_{\text{H}}(R)$  decreases as  $R$  decreases such that  $N_{\text{H}}$  is less than  $N_{\text{H}}^{\text{Gal}}$  near  $R = 0$  for most of the galaxies and groups (§3.1); i.e. excess soft X-ray emission above that produced by the hot gas is significant and is concentrated at the center. Clearly the qualitative features of this trend can be explained by the soft X-ray emission expected from the large masses of the warm gas ( $T \approx (1 - 5) \times 10^5 \text{ K}$ ) implied for the central regions of the systems (Table 2). Due to the limited energy resolution of the PSPC it is virtually impossible to obtain simultaneous constraints on both absorption and emission models for both the warm and hot gas. In particular there is a degeneracy between the oxygen edge optical depth of the warm gas and  $N_{\text{H}}$  of the standard absorber (§3.4) which inhibits constraints on both the absorption and emission model of the warm gas.

The system that suffers least from this degeneracy, and coincidentally has the highest S/N data in the sample (Table 1 of PAPER2), is NGC 5044; i.e.,  $N_{\text{H}}$  of the standard

absorber is well below  $N_{\text{H}}^{\text{Gal}}$  at small  $R$  whether or not an intrinsic oxygen edge is included (Figure 1). If we add a plasma component with  $T \lesssim 0.1$  keV to the spectrum of the central bin of NGC 5044 there is a very noticeable improvement in the fit. In the case of the model with an intrinsic oxygen edge and with  $N_{\text{H}} \equiv N_{\text{H}}^{\text{Gal}}$  for the standard absorber, we find that the addition of the warm plasma component reduces  $\chi^2$  from 156.5 (117 dof) to 129.0 (115 dof). The gas temperature is  $T = 0.035^{+0.053}_{-0.020}$  keV ( $4.1^{+6.1}_{-2.2} \times 10^5$  K) at 90% confidence exactly as expected from the absorption properties (§5.1).

The best-fitting oxygen edge optical depth is  $\tau = 0.83$  which is about half the best-fitting value and near the 95% lower limit of  $\tau$  obtained without including the emission from the warm gas (Table 1). Using this  $\tau$  to compute  $M_{\text{abs}}$  as done in §5.2 we find that the implied emission measure ( $n_{\text{e}} n_{\text{H}} V$ ) of the warm gas agrees exactly with that obtained from the spectral fits. *Hence, the warm gas is required to explain both the excess absorption above  $\sim 0.5$  keV and the excess emission at lower energies in the PSPC data of NGC 5044.*

Emission from such a warm gas component is consistent with, though not as clearly required by, the PSPC data for the other systems. For example, the next best improvement is observed for NGC 4472 where  $\chi^2$  improves from 158.1 (103 dof) to 134.5 (101 dof) when the warm gas component is added to the central bin. Temperatures ( $T \sim (5 - 10) \times 10^5$  K) and the reduction in edge optical depth are obtained similarly as found for NGC 5044 but with large uncertainties.

Future observations with better energy resolution are required to definitively confirm and measure the emission and absorption properties of the warm gas in all of these systems. Assuming the case of NGC 5044 applies generally, then we expect that the absorber masses listed in Table 2 are over-estimates as more realistic values of  $M_{\text{abs}}$  should be near the 95% lower limits. Even considering this effect, the qualitative conclusions regarding cooling flows made in §5.2 still apply.

We mention that systems without strong cooling flows will not have had sufficient time to accumulate the  $\sim 10^9 M_{\odot}$  within  $R \sim 1'$  to produce detectable soft X-ray emission. Thus, the “Very Soft Components” found in galaxies with low ratios of X-ray to optical luminosity unlikely arise from warm gas deposited in a cooling flow and instead probably reflect the collective emission from X-ray binaries (e.g., Irwin & Bregman 1999).

#### 5.4. Implications for other Wavebands

##### 5.4.1. Radio

Warm ionized gas at a temperature of  $10^{5-6}$  K cannot support itself via thermal pressure within the gravitational fields of the galaxies and groups. Magnetic pressure is probably the most viable non-thermal process which can support the gas. It has been known for some time that small seed magnetic fields can be amplified within a cooling flow to produce sizeable fields at the centers (e.g., Soker & Sarazin 1990; Lesch & Bender 1990; Moss & Shukurov 1996; Mathews & Brighenti 1997).

The details of how the magnetic field would support the gas are uncertain. Daines et al (1994) suggest that the cool gas blobs would be anchored to the hot gas by the mag-

netic fields, and thus the pressure support would actually come from the hot gas. However, inspection of Table 2 reveals that  $M_{\text{abs}} \sim (1 - 10) M_{\text{hot}}$  within the central bins indicating that the hot gas could not support the cool gas. At larger radii it may be possible for the hot gas to support the cool gas.

Whatever the details of the magnetic support the condition of hydrostatic equilibrium requires that  $B^2 \sim 6M_{\text{abs}}GM_{\text{grav}}r^{-4}$ . Using the values for  $M_{\text{abs}}$  within the central 1' bin quoted in Table 2 and the gravitating masses obtained from previous *ROSAT* studies (David et al 1995; Kim & Fabbiano 1995; Rangarajan et al 1995; Irwin & Sarazin 1996) we find that  $B \sim 100\mu\text{G}$  is required within a 5 kpc radius.

Estimates of the magnetic field strengths from radio polarization analyses of these galaxies are lacking, although there exist estimates using minimum energy arguments for NGC 1399 (Killeen et al, 1988), NGC 4472 (Ekers & Kotanyi, 1977), and NGC 4649 (Stanger & Warwick, 1986) which give consistent results:  $B \gtrsim 50 - 100\mu\text{G}$  at the centers and  $B \gtrsim (5 - 10)\mu\text{G}$  at  $r \sim 0.5'$ . Assuming  $B \sim r^{-1.2}$  (Mathews & Brighenti, 1997) then these observations imply  $\langle B \rangle \sim 5\mu\text{G}$  when averaged over a 1' circle. Since the observations only set lower limits the expected  $\langle B \rangle \sim 100\mu\text{G}$  fields are consistent with the observations.

Interestingly, the need for  $B \sim 100\mu\text{G}$  in cooling flows has been suggested by Brighenti & Mathews (1997) on entirely different grounds. In their analysis of the gravitating mass distributions of NGC 4472, 4636, and 4649 Brighenti & Mathews (1997) find in every case that the gravitating mass determined from the X-ray analysis falls below that estimated from stellar dynamics for  $r \lesssim (\text{few})\text{kpc}$ . If  $B \sim 100\mu\text{G}$  within the centers of these systems then the X-ray and stellar dynamical masses agree. (A similar result holds for NGC 1399 as well – W. Mathews 2000, private communication.)

##### 5.4.2. Optical and UV

Since collisionally ionized gas at temperatures of  $10^{5-6}$  K emits many strong lines at optical and ultraviolet wavelengths (e.g., Pistinner & Sarazin 1994; Voit & Donahue 1995), we consider whether the large amounts of absorbing material implied by the intrinsic X-ray absorption (Table 2) violate published constraints on line emission in the optical and UV spectral regions. The best published constraints available in the optical are for  $\text{H}\alpha$  from studies of extended ionized gas in the centers of elliptical galaxies (e.g., Trinchieri & di Alighieri 1991; Goudfrooij et al 1994; Macchetto et al 1996). Typically the emission line gas is only detected within  $r \lesssim 20''$  which is significantly smaller than the central 1' used in our analysis.

The object in our sample where  $\text{H}\alpha$  has been detected out to the largest angular radius is NGC 5044. Macchetto et al (1996) measure  $F(\text{H}\alpha) = 1.4 \times 10^{-13} \text{ erg cm}^{-2} \text{ s}^{-1}$  within  $R = 0.5'$ . We can estimate the temperature at which the  $\text{H}\alpha$  emission implied by  $M_{\text{abs}}$  (Table 2) within  $R = 1.0'$  equals the observed flux. We take the predicted  $\text{H}\alpha$  line intensity at peak temperature from Pistinner & Sarazin and the temperature dependence of  $\sim T^{-2.5}$  from inspection of Figure 7 of Voit & Donahue. After accounting for the different region sizes we find that the required temperature is  $\approx 1.5 \times 10^5$  K using the best-fitting  $M_{\text{abs}}$ ,

although when using the 95% lower limit on  $M_{\text{abs}}$  we find that  $T \approx 0.5 \times 10^5$  K.

Similar results hold for NGC 1399, 4472, and 4649 although the comparison is less certain because of the larger aperture corrections. If no aperture correction is made for NGC 5044 then the implied temperatures rise to  $T \approx 2.5 \times 10^5$  K at best fit and  $T \approx 1.7 \times 10^5$  K at the 95% lower limit. If we consider also that  $M_{\text{abs}}$  in Table 2 is over-estimated because the oxygen abundance is larger than solar ( $\sim 1.5Z_{\odot}$  – see PAPER2) and carbon and nitrogen contribute  $\sim 40\%$  to the measured optical depths (§5.2), we obtain  $T \approx 1.8 \times 10^5$  K at best fit and  $T \approx 1.2 \times 10^5$  K at the 95% lower limit (again without aperture correction). Therefore, the published constraints on H $\alpha$  are satisfied if  $T \gtrsim 2.0 \times 10^5$  K.

Stronger lines from warm gas are expected to appear in the UV, but Hopkins Ultraviolet Telescope (HUT) observations detected no significant emission lines in NGC 1399, 4472, and 4649 (Ferguson et al 1991; Brown, Ferguson, & Davidsen 1995). It is unfortunate that the strongest emission lines for temperatures  $T \sim (2 - 3) \times 10^5$  K are O $\text{v}$ (1218Å), O $\text{vi}$ (1034Å), and N $\text{v}$ (1240Å) which are appear to be lost in the background geocoronal emission (e.g., Figure 1 of Ferguson et al 1991, though see below). However, the lines C $\text{iv}$ (1549Å), O $\text{iv}$ (1401Å), and Ne $\text{iv}$ (1602Å) are also strong and uncontaminated by geocoronal emission.

To determine the gas temperature at which, e.g., the O $\text{iv}$ (1401Å) flux would not violate the published UV constraints we estimate that the O $\text{iv}$  flux would have to be less than  $\sim 10\%$  of the continuum considering the error bars on the spectrum of NGC 1399 (Figure 2 of Ferguson et al 1991). This limit corresponds to a flux of  $\sim 1.4 \times 10^{-12}$  erg cm $^{-2}$  s $^{-1}$ . We take the predicted O $\text{iv}$  line intensity at peak temperature from Pistinner & Sarazin and assume the temperature gradient above the peak falls similarly to that displayed for C $\text{iv}$  in Figure 7 of Voit & Donahue. Using the best-fitting  $M_{\text{abs}}$  (and accounting for the smaller HUT aperture) we find that a temperature of at least  $3 \times 10^5$  K is required, though the 95% lower limits on  $M_{\text{abs}}$  (which are probably more realistic – §5.3) coupled with the oxygen abundance and C/N issues as above indicate the limit is more conservatively  $\sim 2 \times 10^5$  K. Similar limits are obtained for the other lines and for the HUT spectra of NGC 4472 and 4649 (Brown et al, 1995).

Our procedure of requiring the line fluxes to be less than 10% of the continuum probably results in limits that are too conservative. Dixon et al (1996) have estimated  $2\sigma$  upper limits on the O $\text{vi}$ (1034Å) intensity from M87 which has a HUT spectrum very similar to NGC 1399. Their  $2\sigma$  upper limit on the O $\text{vi}$  flux within a 1' circle is  $\sim 1 \times 10^{-10}$  erg cm $^{-2}$  s $^{-1}$ . If the warm gas has a temperature of  $3.2 \times 10^5$  K corresponding to the peak temperature for O $\text{vi}$ , then the observed limit is comparable to the O $\text{vi}$  emission expected from the warm gas of NGC 1399 when using the 95% lower limit on  $M_{\text{abs}}$ . Hence, if the HUT results for M87 apply to NGC 1399 (as they appear to), then the predicted O $\text{vi}$  emission agrees with the limits, especially if the temperature is not precisely at the peak temperature for O $\text{vi}$ .

### 5.5. Future Work

Considerable theoretical and observational work is required in order to clarify the nature of the warm ionized gas. Since gas should rapidly cool down to  $T \sim 10^4$  K a theoretical model is needed to explain how the gas remains at  $T \approx (2 - 5) \times 10^5$  K. Perhaps the warm gas represents the outer envelopes of low mass stars forming in a cooling flow as described by Mathews & Brightenti (1999). It is also necessary to understand what non-thermal pressure supports the gas. Magnetic fields could provide the answer, though the required  $\sim 100\mu\text{G}$  fields within  $R = 1'$  seem rather large (§5.4.1). If future radio polarization measurements rule out such large fields, then other non-thermal pressure will need to be considered such as that produced by feedback from the central black hole as advocated by Binney (1996) and Ciotti & Ostriker (2000). Finally, the warm gas clearly extends past the central  $R = 1'$  apertures so inhomogeneous cooling flow models need to make some prediction regarding the density profile of the warm gas.

As discussed in §5.4.2 optical and UV constraints imply a lower limit of  $T \sim 2 \times 10^5$  K. It is possible that precise measurements of O $\text{iii}$ (5007Å) could refine this limit, but since this line peaks at  $T \sim 0.8 \times 10^5$  K its emissivity is already falling rapidly at  $T \sim 2 \times 10^5$  K. If future high resolution UV spectroscopy can distinguish the strong O $\text{v}$  (1218Å) and O $\text{vi}$  (1034Å) lines from the Earth's geocoronal emission then additional constraints on the temperature and mass of the warm gas will be possible. Until that time interesting constraints on the properties of the warm gas will have to come from soft X-ray observations.

We emphasize that the absorption signature of the warm gas is expected to be a relatively broad trough over energies  $0.4 \sim 0.8$  keV, and thus future observations with higher energy resolution than the PSPC will not see a single sharp feature. The most straightforward means to confirm our results will be to reproduce the sensitivity of  $N_{\text{H}}$  to  $E_{\text{min}}$  for a standard absorber model (§3.3). To obtain the properties of the absorber (e.g., temperature and abundances) a model for the soft X-ray opacity such as that described by Krolik & Kallman (1984) must be compared to the new data. In so doing the emission from the warm gas must also be accounted for (§5.3), and thus it is very important that the detector bandpass extend down to  $\sim 0.1$  keV.

The *XMM* (EPIC) and *Chandra* (ACIS-S) CCDs both extend down to 0.1-0.2 keV and have substantially better energy resolution than the PSPC. Observations with these instruments can easily test our prediction for warm gas in both absorption and emission. The grating spectrometers of *XMM* and *Chandra* have even better energy resolution and, in principle, might detect individual edges. This will be difficult because the collecting area for the gratings are relatively small and they are best calibrated for point sources. The  $\sim 10$  eV resolution and sizeable collecting area of the *ASTRO-E* XRS provides the best short-term opportunity to identify individual absorption edges and thus to constrain the properties of the ionized absorber for energies above  $\sim 0.50$  keV.

It should be remembered that to infer the properties of the warm gas from X-ray observations the absorption and emission spectrum arising from warm gas must be disentangled from Galactic absorption and the emission from hot plasma. Since (if confirmed) the warm gas almost certainly represents the mass deposited by an inhomogeneous

cooling flow (§5.2), the hot gas at each radius should also emit over a range of temperatures. Hence, the thermodynamic state of the X-ray emitting plasma appears to be very complex in the central regions of the (X-ray) brightest galaxies and groups, and the analogous results for A1795 presented in PAPER1 suggest the same applies for galaxy clusters.

## REFERENCES

Allen, S. W., & Fabian, A. C. 1997, MNRAS, 286, 583  
 Allen, S. W., Di Matteo, T., & Fabian, A. C., 2000a, MNRAS, in press (astro-ph/9910188)  
 Allen, S. W., Fabian, A. C., Johnstone, R. M., & Nulsen, P. E. J., 2000b, MNRAS, submitted (astro-ph/9910188)  
 Arabadjis, J. S., & Bregman, J. N., 1999, ApJ, 514, 607  
 Balucińska-Church, M., & McCammon, D., 1992, ApJ, 400, 699  
 Binney, J., 1996, in Gravitational Dynamics Proc. 36th Herstmonceux conf., ed O. Lahav (Cambridge: Cambridge University Press), 89  
 Bregman, J. N., Hogg, D. E., & Roberts, M. S., 1992, ApJ, 387, 484  
 Briel, U. G., & Henry, J. P., 1996, ApJ, 472, 131  
 Brightenti, F., & Mathews, W. G., 1997, ApJ, 486, L83  
 Brightenti, F., & Mathews, W. G., 1998, ApJ, 495, 239  
 Brown, T. M., Ferguson, H. C., Davidsen, A. F., 1995, ApJ, 454, L15  
 Buote, D. A., 1999, MNRAS, 309, 695  
 Buote, D. A., 2000a, MNRAS, 311, 176  
 Buote, D. A., 2000b, ApJLetters, submitted (PAPER1)  
 Buote, D. A., 2000c, ApJ, submitted (PAPER2)  
 Buote, D. A., & Fabian, A. C. 1998, MNRAS, 296, 977  
 Ciotti, L., & Ostriker, J. P., 2000, ApJ, submitted (astro-ph/9912064)  
 Daines, S. J., Fabian, A. C., & Thomas, P. A., 1994, MNRAS, 268, 1060  
 Daltabuit, E., & Cox, D. P., 1972, ApJ, 177, 855  
 David, L. P., Jones, C., Forman, W., Daines, S., 1994, ApJ, 428, 544  
 Dickey J. M., Lockman F. J., 1990, ARA&A, 28, 215  
 Dixon, W., Hurwitz, M., & Ferguson, H. C., 1996, ApJ, 469, L77  
 Ekers, R. D., & Kotanyi, C. G., 1977, A&A, 67, 47  
 Fabian A. C., 1994, ARA&A, 32, 277  
 Fabian, A. C., Arnaud, K. A., Bautz, M. W., & Tawara, Y., 1994, ApJ, 436, L63  
 Ferguson, H. C., et al, 1991, ApJ, ApJ, 382, L69  
 Forman W., Jones C., David L., Franx M., Makishima K., & Ohashi T., 1993, ApJ, 418, L55  
 Goudfrooij, P., Hansen, L., Jorgensen, H. E., & Norgaard-Nielsen, H. U., 1994, A&AS, 105, 341  
 Gould, R. J., & Jung, Y.-D., 1991, ApJ, 373, 271  
 Ikebe Y., et al., 1997, ApJ, 481, 660  
 Irwin, J. A., & Bregman, J. N., 1999, ApJ, 527, 125  
 Irwin, J. A., & Sarazin, C. L., 1996, ApJ, 471, 663  
 Johnstone R. M., Fabian A. C., Edge A. C., & Thomas P. A., 1992, MNRAS, 255, 431  
 Jones, C., Stern, C., Forman, W., Breen, J., David, L., Tucker, W., & Franx, M., 1997, ApJ, 482, 143  
 Killeen, N. E. B., Bicknell, G. V., & Ekers, R. D., 1988, ApJ, 325, 180  
 Kim, D.-W., & Fabbiano, G., 1995, ApJ, 441, 182  
 Krolik, J. H., & Kallman, T. R., 1984, ApJ, 286, 366  
 Lesch, H., & Bender, R., 1990, A&A, 233, 417  
 Lester, D. F., Zink, E. C., Doppmann, G. W., Gaffney, N. I., Harvey, P. M., Smith, B. J., & Malkan, M., 1995, ApJ, 439, 185  
 Macchietto, F., Pastoriza, M., Caon, N., Sparks, W. B., Giavalisco, M., Bender, R., & Capaccioli, M., 1996, A&AS, 120, 463  
 Mathews, W. G., & Brightenti, F., 1997, ApJ, 488, 595  
 Mathews, W. G., & Brightenti, F., 1999, ApJ, 526, 114  
 Morrison, R., & McCammon, D., 1983, ApJ, 270, 119  
 Moss, D., & Shukurov, A., 1996, MNRAS, 279, 229  
 Nahar, S. N., 1999, ApJS, 120, 131  
 Nahar, S. N., & Pradhan, A. K., 1997, ApJS, 111, 339  
 O'Dea, C. P., Baum, S. A., Maloney, P. R., Tacconi, L. J., Sparks, W. B., 1994, ApJ, 422, 467  
 Pisterne, S., Sarazin, C. L., 1994, ApJ, 433, 577  
 Rangarajan, F. V. N., Fabian, A. C., Forman, W. R., & Jones, C., 1995, MNRAS, 272, 665  
 Sarazin, C. L., Wise, M. W., Markevitch, M. L., 1998, ApJ, 498, 606  
 Snowden, S. L., McCammon, D., Burrows, D. N., & Mendenhall, J. A., 1994, ApJ, 424, 714  
 Soker, N., & Sarazin, C. L., 1990, ApJ, 348, 73  
 Stanger, V. J., & Warwick, R. S., 1986, MNRAS, 220, 363  
 Sutherland, R. S., & Dopita, R. S., 1993, ApJS, 88, 253  
 Thomas P. A., Fabian A. C., & Nulsen P. E. J., 1987, MNRAS, 228, 973  
 Trinchieri, G., & di Serego Alighieri, S., 1991, AJ, 101, 1647  
 Trinchieri G., Fabbiano G., Kim D.-W., 1997, A&A, 318, 361  
 Trinchieri G., Kim D.-W., Fabbiano G., & Canizares C., 1994, ApJ, 428, 555  
 Tsai, J. C., & Mathews, W. G., 1995, ApJ, 448, 84  
 Tsai, J. C., & Mathews, W. G., 1996, ApJ, 468, 571  
 Voit, G. M., & Donahue, M., 1995, ApJ, 452, 164  
 White, D. A., Fabian A. C., Johnstone R. M., Musthotzky, R. F., & Arnaud, K. A., 1991, MNRAS, 252, 72  
 Xu H., Makishima K., Fukazawa Y., Ikebe Y., Kikuchi K., Ohashi T., & Tamura T., 1998, ApJ, 500, 738